BULLETIN OF THE POLISH ACADEMY OF SCIENCES
TECHNICAL SCIENCES, Vol. 73(1), 2025, Article number: e151952
DOI: 10.24425/bpasts.2024.151952

The influence of brace to chord rotational connection stiffness on stability of the truss

Marcin KRAJEWSKI

Gdansk University of Technology, Faculty of Civil and Environmental Engineering, Department of Structural Mechanics, Poland

Abstract. The paper is devoted to numerical analysis of the roof truss subjected to upward wind loading and braced at the tensioned top chord. Linear buckling analysis was performed for the beam and shell model of the structure. As a result, the influence of rotational connection stiffness between the brace and the top chord on truss stability was noted. A bi-axial strength testing machine was used to conduct the experimental tests of the rotational connection stiffness between selected steel profiles. The results in the form of measured structural displacements and rotations were presented. The static nonlinear analysis results obtained for the shell model of the structural connection were compared to the results obtained on the experimental set-up.

Keywords: truss; stability; connection; rotational stiffness.

1. INTRODUCTION

Flat trusses are often designed as roof girders in large-span civil engineering buildings. The characteristic feature of that type of structures is high stiffness and load bearing capacity but only in their plane. In the perpendicular direction (out-of-plane), the braces are designed to ensure truss stability. There are many types of bracing systems described in literature. The main role of these lateral supports is to restrain the out-of-plane deformations of the roof structure. The braces are designed (among others) to carry the horizontal load caused by wind. However, it should be pointed out that these elements are also subjected to the so-called imperfection load [1,2]. This horizontal load results from the vertical load being subjected to imperfect truss. In this case, load magnitude depends on the distribution of normal forces in the compressed chord [3–5] and on the imperfection shape of the girder [6].

In many cases in order to simplify the design process, the braces are assumed to be rigid. As a consequence, the buckling length of the compressed top chord (for the gravity load) or bottom chord (for the wind suction) is assumed as a distance between the lateral supports. The lattice failure (buckling at the bottom chord) caused by the wind was the subject of analysis presented in [7]. Studies on the influence of elastic brace stiffness on truss stability were performed numerically [8–11] and experimentally [12–14]. In these studies, the steel structures described by different geometry, cross-section types and boundary conditions were considered. Also the brace translational (out of plane, k) and rotational stiffness (k_{rot}) was taken into account. As one of the results the relation between the external loads and the truss top chord translations (out of plane) and rotations (torsion) was obtained. Moreover, it is worth noting that truss capacity was also dependent on initial geometric imperfections [15,16].

Based on the analytical solutions presented in [17], it can be concluded that a properly designed connection between the brace and the top chord significantly affects the structure bearing capacity. In the case of wind loading, the diagonals are the natural intermediate supports for the compressed bottom chord. These elements can be treated as the elastic foundation for the compressed element. However, in this case the bottom chord buckling length does not depend solely on bending stiffness (out-of-plane) of the diagonals and torsional stiffness of the tensioned top chord. It depends also on brace rotational stiffness. Rotational stiffness of the truss side supports results from the bending stiffness of the purlin and rotational connection stiffness between the purlin and the top chord [17] (1).

$$\frac{1}{k_{\text{rot}}} = \frac{1}{K_{\text{roof}}} + \frac{1}{K_{\text{con}}}, \tag{1}$$

where: k_{rot} – rotational stiffness of lateral support, K_{roof} – bending stiffness of the brace, K_{con} – rotational connection stiffness between the brace and the truss top chord.

As appears from the results of numerical analysis, rotational brace stiffness affects the imperfection load (horizontal stabilizing forces) mentioned above [6]. The research on the connection stiffness between the steel roof profiles and the trapezoidal sheeting, including the design details implementation in the numerical model, were presented in [18].

The present paper is focused on stability studies of the braced truss. The structure presented previously in [17] was taken into consideration. However, the continuous braces along the top chord length (corrugated sheet) were replaced with the lateral point supports located at selected nodes. The truss subjected to upward wind loading was taken into account. The analysis was conducted for the structure without any additional braces located at the compressed bottom chord. Rotational stiffness for

*e-mail: markraje@pg.edu.pl

Manuscript submitted 2024-03-28, revised 2024-06-17, initially accepted for publication 2024-08-27, published in January 2025.

the selected connection type (brace to chord) was tested experimentally, which constitutes the main part of the research presented herein. The results obtained on the prototype experimental set-up were used to validate the numerical (shell) models of the structural connection. Based on numerical analysis results, the influence of brace rotational stiffness on the truss buckling load was presented.

2. DESCRIPTION OF THE TESTED STRUCTURES

2.1. Numerical model of the truss

The model of a steel flat truss loaded at braced top chord joints was taken into consideration (Fig. 1). The analysis of a similar structure was presented previously in [17], however in the current parametrical studies the braces in the form of elastic point supports (purlins) were taken into account instead of a bracing system in the form of a trapezoidal sheet. The truss length was $L = 15.0$ m and the depth stood at $h = 0.7$ m. Individual members of the structure were made of rectangular bars: top chord – RHS $120 \times 100 \times 4$, bottom chord – RHS $100 \times 100 \times 4$, diagonals – RHS $50 \times 50 \times 3$. The truss was made of S355 steel. Based on the standard requirements [1], the following material parameters were assumed: Young's modulus $E = 210$ GPa, Poisson's ratio $\nu = 0.3$ and the yield strength of the steel $f_y = 355$ MPa.

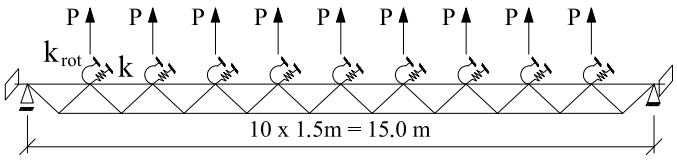

Fig. 1. Static schema

The finite element method was used to perform stability analysis for the spatial (beam and shell) models of the structure defined in *Femap with NX Nastran* software [19] (Fig. 2). About 400 beam elements with six degrees of freedom at node were used. The truss elements were connected at joints by means of rigid links. The load (upward wind loading) was applied in the form of concentrated forces located at the top chord braced joints. The braces (purlins) were modeled in the form of side supports (*Dof-spring* elements [19]) characterized by translational (k) and rotational stiffness (k_{rot}).

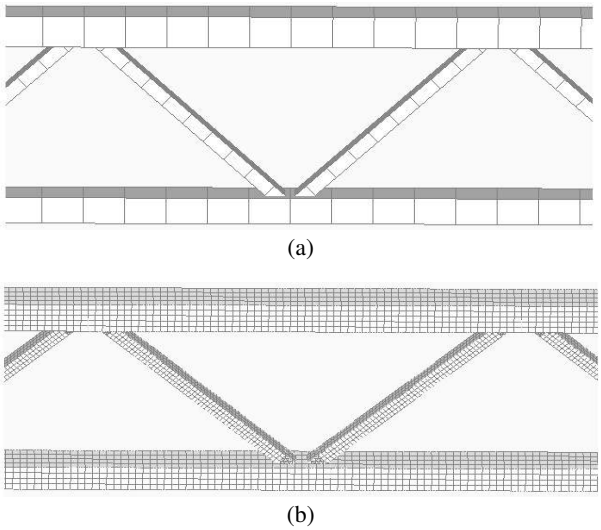

(a)

(b)

Fig. 2. Numerical model details: (a) beam model, (b) shell model

The shell model of the structure was created on the basis of a detailed design project. In this case about 34 000 4-node shell elements (*Quad4* [19, 20], six degrees of freedom at node, one Gauss point) were used. All eccentric connections between the separated truss members were taken into account. The rigid elements were defined as the replacement for welded connections between diagonals and chords.

The model of the truss was loaded and supported at the selected top chord joints. In this case the intermediate (lateral) and marginal supports and also the concentrated forces were applied to the nodes defined in the center of gravity of the RHS $120 \times 100 \times 4$ profile. These reference nodes were rigidly connected with the selected nodes located around the cross-section perimeter of the rectangular bar.

It the present research, it was assumed that the intermediate supports were rigid by means of out of the truss plane translation ($k = 10^6$ kN/m). In the parametric studies, the influence of rotational brace stiffness (k_{rot}) on the truss buckling load was considered. The structure with two different variants of the bracing system was taken into account. In the first case, each top chord joint was braced (distance between the braces was $L_{br} = 1.5$ m). In the second case, the distance between the marginal supports and braces and also the distance between the braces was equal to $L_{br} = 3.0$ m. The truss was pinned at the marginal supports.

Before the target numerical analysis started (linear buckling analysis, solving the matrix eigenvalue problem), both the above-described models of the truss were calibrated by means of mesh density. As the first step, each separated member of the structure was divided into two parts (beam model – model A). In the next step, 10 finite elements per member were used (Fig. 2a, model B). In the last step, 100 finite elements were applied (model C). As appears form the analysis results, the differences in buckling load magnitudes were less than 5% when models B and C were compared. On this basis, the target analysis was performed for model B of the truss (Fig. 2a). Similar research was carried out for the shell model of the structure. In this case, as the first step the rectangular profiles were divided into 2 finite elements along cross-section height and depth. In the next step (mostly), the dimensions of square elements were about 20×20 mm (Fig. 2b). The shell model of the truss built of 5.0×5.0 mm square elements was also tested. Based on the results obtained, the model presented in Fig. 2b was chosen to perform stability analysis for the shell structure.

2.2. Details about the tested structural connection

The connection between the truss top chord and the purlin was taken into consideration. In this case, the experimental tests and numerical analysis of the connection stiffness between the RHS $120 \times 100 \times 4$ profile (part of the truss top chord, S355, length $L_{ch} = 1.5$ m) and IPE100 (part of the purlin, S355, length $L_p = 0.75$ m) were performed. The middle of the I-beam was

located in the middle of the rectangular bar. The contoured gusset plates (S275, thickness 4.0 mm, located at both sides of the I-beam) and screws (M8, 8.8 class) were used to enable the connection between the main profiles situated one on top of the other (Fig. 3, Fig. 4).

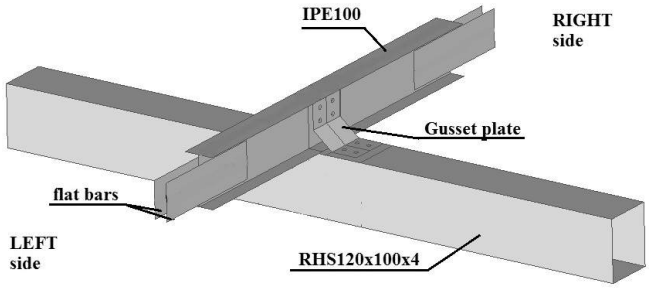

Fig. 3. Structural connection

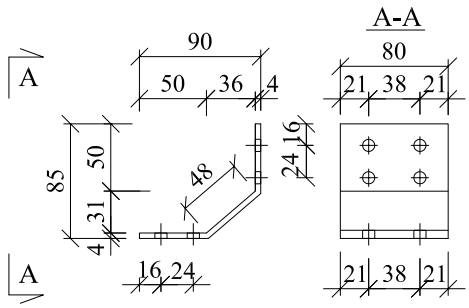

Fig. 4. Gusset plate detail

The bi-axial strength testing machine [21] was used to conduct the experimental tests. In each case the sample was situated on the experimental set-up at the initial angle $\alpha = 10°$ (Fig. 5). Both ends of the RHS $120 \times 100 \times 4$ profile were fixed to the additionally designed steel frames. Loading was applied (at the same time) to both ends of the I-beam. The steel handles attached to the moving travers (at both opposite sides) were used to combine the tested specimen with the machine (Fig. 6). The handles were pinned to the flat bars, which were connected with the IPE100 profile. The distance between the hinges was $L_b = 0.93$ m.

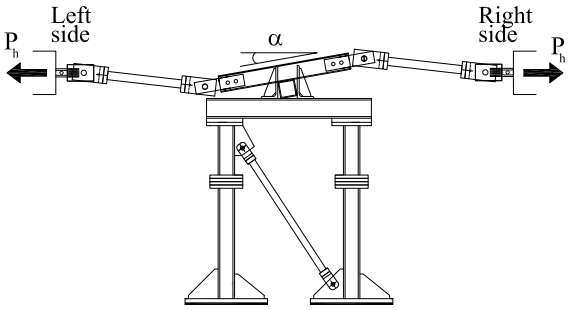

Fig. 5. Sample test positioning and load application

Based on the loading schema (Fig. 7), one can conclude that during the experiment the samples were subjected to tension and bending. It is worth noting that rotational stiffness of the

Fig. 6. Experimental set-up

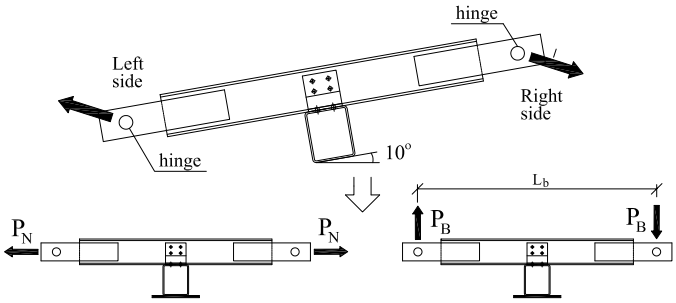

Fig. 7. Load application details

connection between the rectangular bar and the I-beam was obtained based on the load corresponding to bending. The four samples were tested experimentally. The maximum applied horizontal load (P_H, Fig. 5) indicated by the machine force gauges was 18 kN. According to the loading procedure at the first step of the experiment, the samples were loaded up to 1.0 kN. In the next step, the load decreased to 0.5 kN. In each case this process was needed to avoid the gaps between the set-up components. In the next stage, the target measurements started and the test speed was 1.0 kN/min.

During the test, the horizontal displacements of the travers (independently at both ends, Fig. 5) and the applied load were all recorded by the strength testing machine devices [21]. The rotation angle of the sample was also measured by the inclinometers [22] connected to the recording devices [23]. The inclinometers were situated at a distance of 0.15m from the ends of the I-beam (Fig. 8). Measurement frequency was 50 Hz and accuracy stood at 0.01 degree.

Fig. 8. Inclinometers location on the tested specimen

For selected points located on the tested structure the strains were also measured. The strain gauges (Sg1–Sg4) were located in the middle of the I-beam web and also in the middle of the top

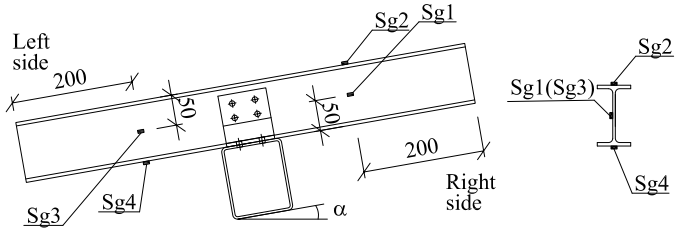

Fig. 9. Location of strain gauges (Sg1–Sg4) on the purlin

or bottom shelf of the profile (Fig. 9). The sensors were installed at both profile ends (on the left connection side and on the right side). In this case the recording amplifier [24] was used and measurements frequency was 50 Hz. With the results obtained from the sensors, the bending load (P_B) and tensile load (P_N) subjected to the tested sample could also be obtained. In this case the calculations were made on the basis of (2) and (3) for the sensors located on the right side of the connection (ε_1 from Sg1, ε_2 from Sg2). In order to determine the load magnitudes (P_B, P_N) on the left side, strains ε_3, ε_4 (from Sg3 and Sg4, respectively) were taken into account.

$$P_N = EA\varepsilon_1 \tag{2}$$

where: P_N – load corresponding to sample tension (on the right side), E – Young's modulus, A – cross-section area of the I-beam, ε_1 – strains measured by Sg1 strain gauge.

$$P_B = \frac{EW}{L_{Sg}}(\varepsilon_2 - \varepsilon_1), \tag{3}$$

where: P_B – load corresponding to sample bending (on the right side), W – moment of cross-section resistance, L_{Sg} – distance between the hinge and strain gauge Sg1 (0.29 m), ε_2 – strains measured by Sg2 strain gauge.

The finite element method was used to perform static non-linear analysis [25] for the tested structure. About 11 000 shell elements (*Quad* [19, 20], three and four node elements with six degrees of freedom at node and one Gauss point) were used to define the separate members of the structural connection (Fig. 10). In most cases the element side length was up to 0.01 m along the walls of the steel profiles and gusset plates. The rigid elements (handles) were implemented in the numerical model as the connection between the tested specimen and the strength testing machine servomotor. The pinned supports with the possibility of sliding (in the horizontal direction) were modeled on one of the ends of the above-mentioned rigid elements. On the other side, due to the design project, the connection between the handles and the flat bars (joined with a IPE100 profile) was pinned (Fig. 5). In the numerical model, the load in the form of concentrated forces was introduced. These horizontal forces (with opposite turns) were applied to the supports described above. The structure was also supported in perpendicular direction. In this case, in the first step the rigid links [19] were modeled between the walls of the rectangular bar and the node located at the center of gravity of the profile (at both profile ends). In the next step, the fixed supports were defined in these two reference nodes. It should also be pointed out that in the numerical analysis the contact surfaces were taken into account. Friction was defined between the bottom shelf of the IPE100 and the top shelf of the RHS $120\times100\times4$. Also the connection was defined between the gusset plates and the profiles mentioned above. The assumed kinematic friction coefficient was equal to 0.5. In the numerical model, the separate members of the structure were also connected by means of beam elements (circular bar elements, diameter 8 mm, six degrees of freedom at node [19]) located at the holes for bolts. In the analysis, the bi-linear elasto-plastic steel model [25] was taken into account (E, f_y due to the standard requirements [1]).

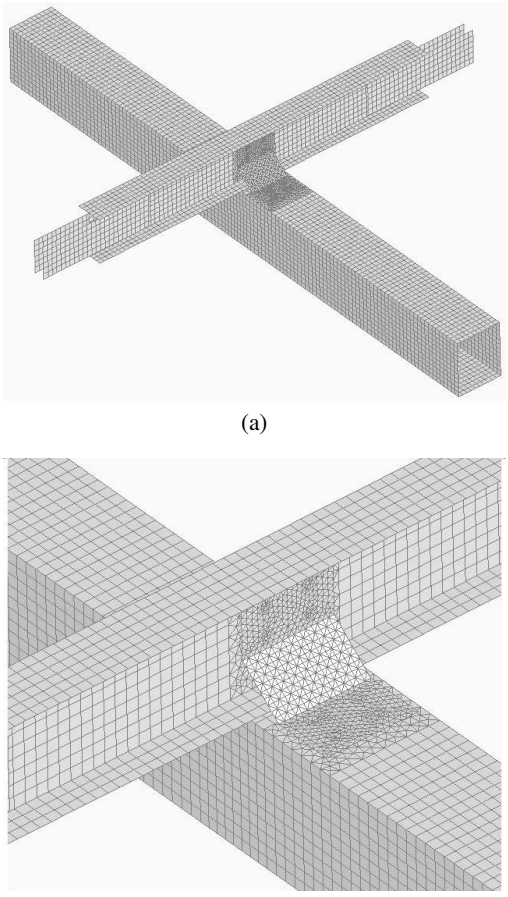

(a)

(b)

Fig. 10. Shell model of the connection: (a) general view, (b) detail of the gusset plate

3. ANALYSIS RESULTS

3.1. Numerical analysis results for the truss

Linear buckling analysis (LBA) was performed for the beam and shell model of the structure. The truss was loaded and braced ($k = 10^6$ kN/m and k_{rot}) in every top chord node (variant I, $L_{br} = 1.5$ m) or in every second top chord node (variant II, $L_{br} = 3.0$ m). As a result, the buckling load and the corresponding buckling modes were obtained (Fig. 11, Fig. 12, Fig. 13). Based on the results, one can conclude that the magnitude of load depended on the rotational stiffness of the lateral supports. In most cases the increase of brace stiffness caused the increase of

buckling load. However, there was the threshold brace stiffness above which the load did not increase or load increase was small (less than 10%). For the tested structure this threshold rotational stiffness of the side supports was equal to 75 kNm/deg (for the beam or shell model).

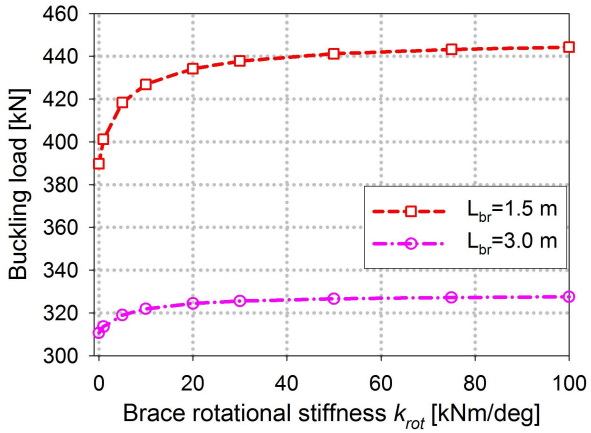

Fig. 11. Relation between the buckling load and the brace rotational stiffness for the beam model (with respect to distance between the lateral supports, L_{br})

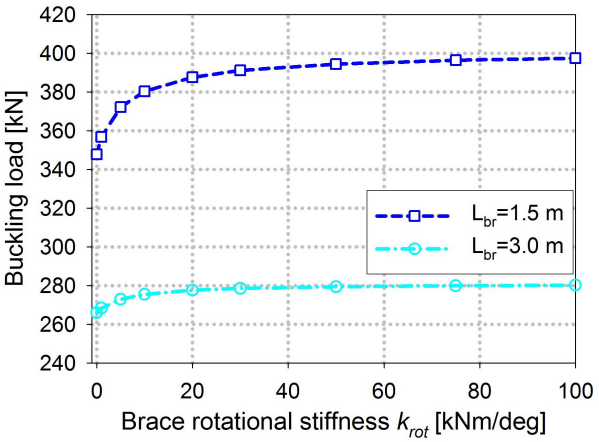

Fig. 12. Relation between the buckling load and the brace rotational stiffness for the shell model (with respect to distance between the lateral supports, L_{br})

Moreover, it is worth noting that the compressed bottom chord did not buckle in one half-wave (Fig. 13) even if the rotational brace stiffness was omitted (top chord braces rigid for out of plane translation, $k = 10^6$ kN/m and $k_{\text{rot}} = 0$ kNm/deg). This means that for the tested structure (without any additional supports located at the bottom chord), buckling length of the bottom chord was in each case (beam or shell models) lower than the length between the marginal supports. The buckling mode in the form of one half-wave at the compressed chord appeared only if brace translational stiffness was $k < 100$ kN/m (and $k_{\text{rot}} = 0$ kNm/deg, $L_{br} = 1.5$ m). Similar analysis results performed for the steel flat trusses were presented previously in [10, 11, 14]. Stiffness of the diagonals (out-of-plane) also affects the buckling length of the bottom chord [17]. These elements supported by the top chord were the elastic foundation for the compressed bottom chord. In this case also the closed cross-section shape of the top and bottom chord (torsional stiffness) had a significant influence on the magnitude of the buckling load in comparison to the structures made of profiles with built-up or opened cross-section [14, 15].

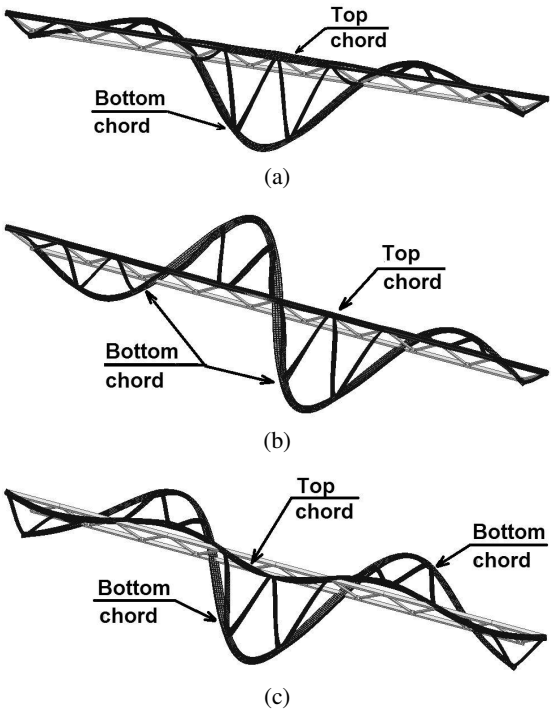

Fig. 13. Buckling modes of the truss (shell or beam models) with braces of stiffness ($k = 10^6$ kN/m): (a) $k_{\text{rot}} = 0$ kNm/deg, $L_{st} = 1.5$ m, (b) $k_{\text{rot}} = 10^6$ kNm/deg, $L_{st} = 1.5$ m, (c) $k_{\text{rot}} = 0$ kNm/deg or $k_{\text{rot}} = 10^6$ kNm/deg, $L_{st} = 3.0$ m

In the present research the buckling load grew up to 12% for the shell model or 13% for the beam model due to the increase in rotational support stiffness. It should be pointed out that the greatest increase in buckling load occurred for the low magnitudes of rotational support stiffness. The maximum load magnitude obtained for the shell model of the truss was about 10% lower in comparison to the beam model. In this case the reason for the discrepancies were the differences in structural details modeling (e.g. diagonal to chord connections, boundary conditions) described in the previous section.

3.2. Experimental and numerical analysis results for the tested structural connection

The main purpose for conducting the experimental research was to determine the angle of rotation for the tested I-beam (supported by the rectangular bar) caused by the application of horizontal forces. Based on the obtained results, validation of the numerical shell model was carried out and in the next step rotational connection stiffness was calculated. In each case the increase of load caused the increase of horizontal displacements of the tested structure (with handles, Fig. 14, Fig. 15).

A further research result which was observed on the experimental station was the decrease of the initial rotation angle of

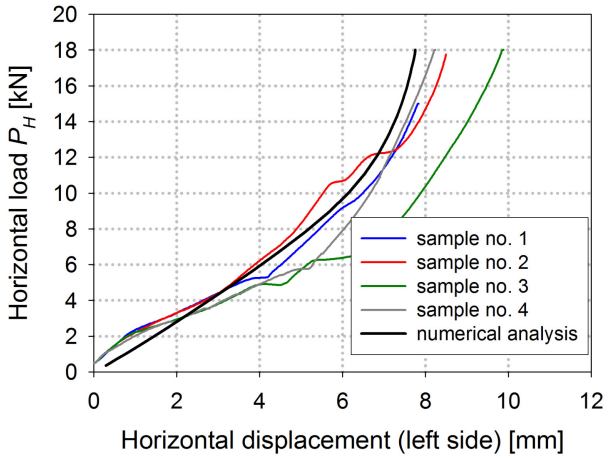

Fig. 14. Relation between the horizontal load (P_H) and the horizontal displacements measured on the end of the handle on the left side of the experimental set-up

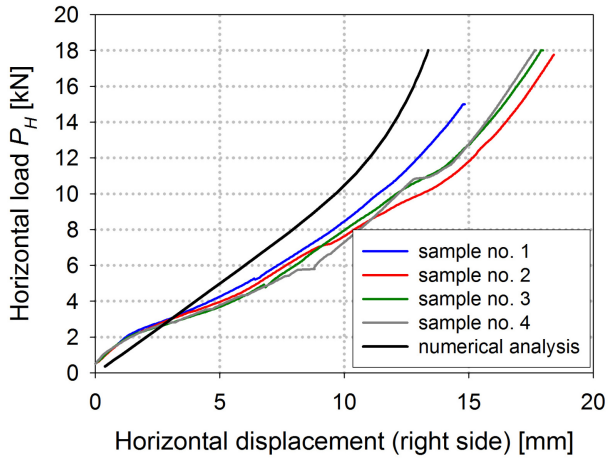

Fig. 15. Relation between the horizontal load (P_H) and the horizontal displacements measured on the end of the handle on the right side of the experimental set-up

the sample (10 deg), caused by the load implementation. Before the tests started, the values measured by the inclinometers were set to zero and therefore the raise of the rotation angle was recorded during the experiment (Fig. 16). As the load increased, the I-beam and the handles became straightened to each other. However, based on the presented results, even for the highest load magnitude (18 kN) the I-beam did not reach the horizontal position and the rotation angle was up to 6.0 deg.

During the experiment, the stresses obtained on the left and right side of the I-beam (based on strains, Fig. 9) grew due to the increase of horizontal load (P_H). These values measured at the maximum load level did not exceed the yield strength of the steel. The load applied perpendicularly to the longitudinal axe of the I-beam (bending load, P_B) and also the tensile load (parallel to the longitudinal axe of the I-beam, P_N, Fig. 7) were calculated on the basis of the measured strains in accordance with (2) and (3). At the same time, the rotation of the I-beam was measured. In this case, the relation between the bending

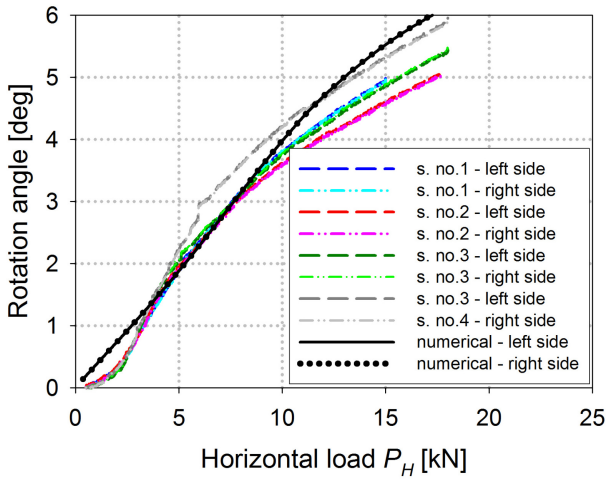

Fig. 16. Relation between the angle (φ) of the I-beam rotation measured on the left or right side of the profile and the horizontal load (P_H) (experimental and numerical analysis results)

load or the tensile load (acting on the left or the right side of the specimen) and the rotation of the I-beam was calculated (Fig. 17, Fig. 18). On this basis, the relation between the bending moment ($M = P_B L_b$, averaged bending load on the left and ride side of the connection) and angle of the rotation (φ) was determined (Fig. 19).

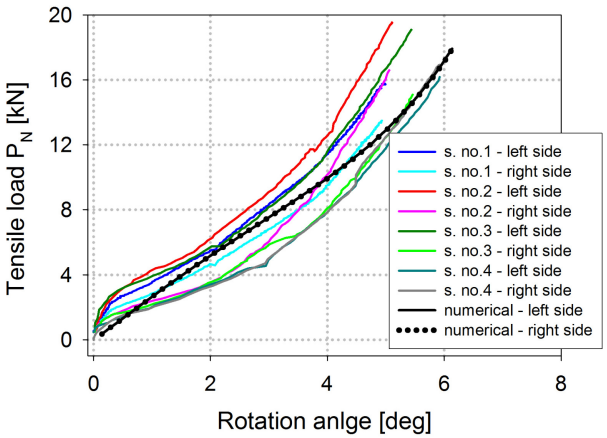

Fig. 17. Relation between the tensile load (P_N, measured on the left or right side of the tested sample) and the angle (φ) of the I-beam rotation (experimental and numerical analysis results)

Due to the method of load transformation from the strength testing machine to the sample, the increase of bending load was non-linear. Under the highest horizontal loads (caused by the machine servomotors), the increase in bending load was the lowest, which was significantly influenced by the angle of sample rotation (Fig. 18).

Moreover, it should be pointed out that at the beginning of the experiment there was the contact surface between the walls of the steel profiles (between the bottom shelf of the I-beam and the top wall of the rectangular bar). However, during the experiment, left side of the I-beam (Fig. 5) was lifted relatively to the rectangular bar and the right side was pressed against the

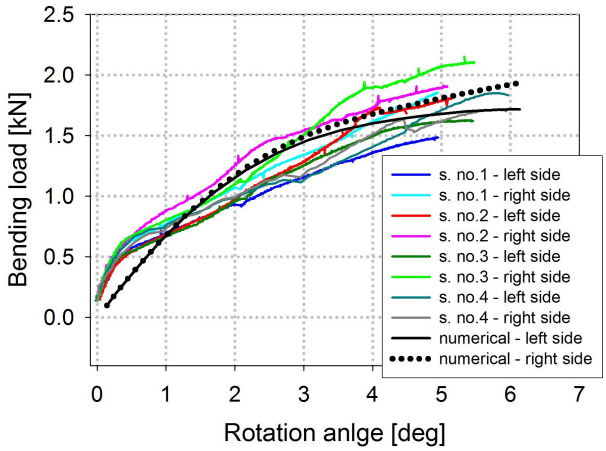

Fig. 18. Relation between the bending load (P_B, measured on the left or right side of the tested sample) and the angle (φ) of the I-beam rotation (experimental and numerical analysis results)

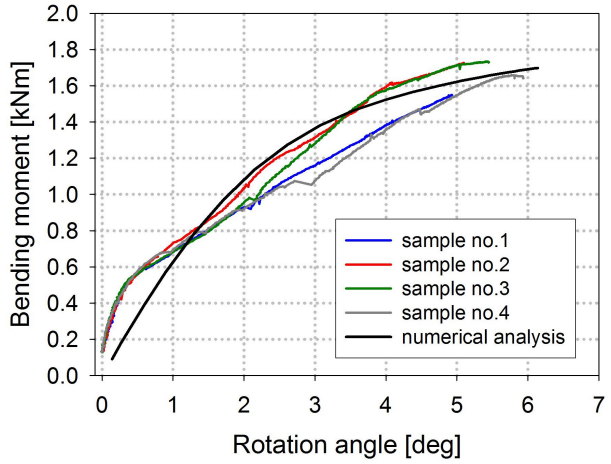

Fig. 19. Relation between the bending moment (M) and the angle (φ) of the I-beam rotation (experimental and numerical analysis results, gusset plates thickness 4 mm)

bar. This was the reason for the increase of the gap between the separated profiles due to the increase of the load. On this basis, during the tests the bottom shelf of the I-beam was connected only to the edge between two perpendicular walls of the tube (by the right side of the connection). In this case, the support line for the IPE100 profile was formulated. On this basis, one can conclude that the distance between the support line (mentioned above) and the bending force on the left side of the I-beam was greater in comparison to the corresponding distance on the right side. That is the possible explanation for the slight differences in load components (bending load) on the left and right side of the connection (Fig. 18). Moreover, the geometric imperfections (caused by element assembly, not included in the numerical model) might affect the experimental results obtained (Fig. 17, Fig. 18).

Due to the load application, the gusset plates connected with the steel profiles by several bolts (Fig. 3, Fig. 4) were subjected to tension on the left side of the connection and to compression on the right side. During the tests, the shearing of the screws was not noticed in all instances. It was observed that both steel sheets were deformed symmetrically in relation to the I-beam (Fig. 20). Due to the limited capabilities of the machine [21] in terms of the maximum load level, the gusset plates used for the experimental tests were made of thin 4 mm sheets. In this case, based on the numerical analysis results the stresses equal to the yield stress of the steel (f_y = 275 MPa, [1]) appeared on the outer (tensioned) edge of the gusset plates for the horizontal load equal to 4 kN.

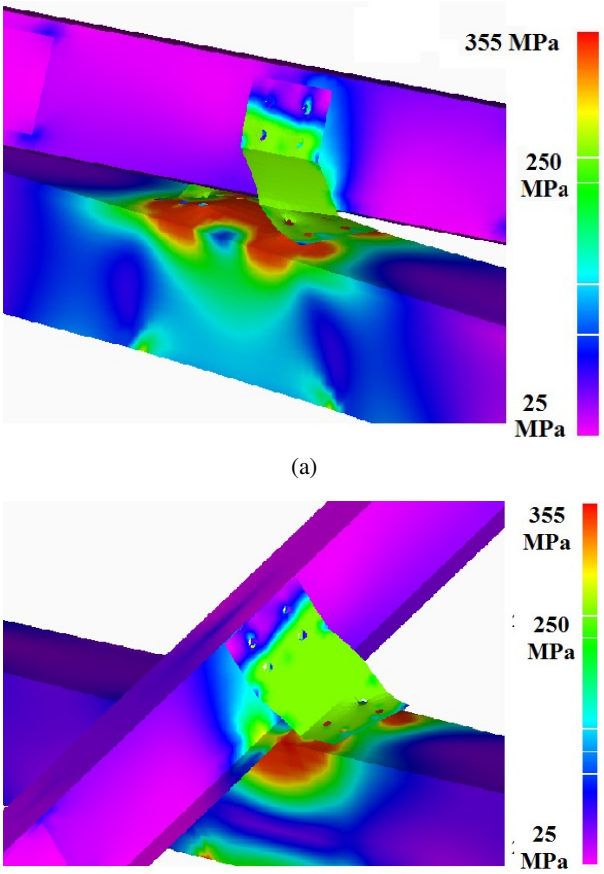

Fig. 20. Deformation and the stress state (HMH hypothesis, top surface of the shell model element) at the limit load for the structural connection: (a) view form the left side, (b) view from the right side

According to the results presented in Fig. 19, linear approximation was provided for each of the four samples (for the limited load range from 0.6 kNm to 1.6 kNm). Based on these calculations, averaged rotational connection stiffness (constant, $K_{\text{con}} = M/\varphi$) equal to about 0.3 kNm/deg was obtained. However, it should be pointed out that this stiffness magnitude was found experimentally assuming that both the I-beam and the rectangular bar were flexible. In order to determine the rotational connection stiffness described in (1), further analyses were taken into consideration. In the next step, it was assumed that both the steel profiles mentioned above were rigid. In this case, based on the nonlinear analysis results (GMNA), performed for the validated shell model of the structural connection (gusset plates

4 mm thickness), rotational stiffness equal to 2 kNm/deg was obtained. However, this stiffness magnitude was calculated for the low range of the rotation angle (up to 0.5 deg, Fig. 21). For the larger angles stiffness decreased. Based on the numerical analysis results (Fig. 21), the increase of gusset plates thickness did not result in significant changes of connection stiffness. The average stiffness of the connection was equal to about 1 kNm/deg for the steel sheets of 5 mm in thickness (up to the rotation angle equal to 2 deg) and 6 mm in thickness (up to the rotation angle equal to 2.5 deg). In this cases, similarly to the gusset plates tested experimentally, for larger rotation angles the connection stiffness decreased. Based on the numerical analysis results (LBA), the truss buckling load grew up to 3% due to the implementation of the side supports of stiffness equal to k_{rot} = 1.0 kNm/deg (in comparison to the pinned connection).

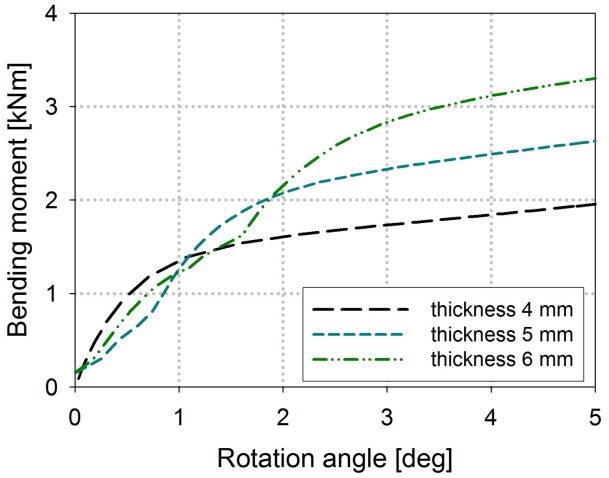

Fig. 21. Relation between the bending moment (M) and the angle (φ) of the I-beam rotation relative to the rectangular bar (both rigid profiles) with respect to the thickness of the gusset plates

4. CONCLUSIONS

In the present research, the model of a braced roof truss was taken into consideration. On the basis of results of numerical analysis (LBA), conducted for the beam and shell model of the structure, one can conclude that the buckling load depended on brace rotational stiffness. In most cases the buckling load raised due to the increase of side support stiffness. However, there was the threshold brace stiffness above which the load did not increase or the increase was low (less than 10%). The critical load obtained for the shell model of the truss was about 10% lower in comparison to the beam model (rigid braces). In this case the possible explanation were the differences in modeling of structural details (boundary conditions, connections between separated members). On the basis of buckling modes, one can conclude that the buckling length of the compressed bottom chord was in each case lower than the length between the marginal supports. The brace stiffness and the bending and torsional stiffness of the diagonals and top chord (closed cross-sections) significantly influenced the magnitude of the truss buckling load.

The experimental tests results and numerical analysis results (shell model, GMNA) obtained for the described structural connection were comparable. The reason for the discrepancies might be the boundary conditions applied to the section of the upper chord in numerical analysis (fixed supports at both ends of the rectangular bar). Also in the numerical model the initial geometric imperfections of the tested steel profiles, including assembly conditions, were not taken into account.

Based on the obtained results, it can be concluded that significant deformations occurred on gusset plates. Due to the increase of load, the plasticization range appeared and raised on the surface of these elements. Moreover, it should be pointed out that during the tests not only the I-beam but also the rectangular bar was subjected to displacements and rotations. The length of the tested section of the top chord had a significant impact on the amount of deformation. Validation of the numerical models was performed due to the experimental test results. On this basis, rotational connection stiffness between the brace and the chord was determined. As can be concluded from the numerical analysis results, the increase of thickness of the gusset plates did not result in the increase of connection stiffness. However, rotational stiffness of the tested connection influenced truss stability.

The use of two-axis strength testing machines enabled the experimental tests. However, the load could only be applied in the limited range and the size of the samples had to be limited.

The next research step is to carry out the process of optimization in terms of stiffness and load bearing capacity for that type of connections. Appropriate connection stiffness between the purlin and the top chord determined during the design process may affect the reduction of additional braces located at the compressed bottom chord of trusses subjected to wind loading.

ACKNOWLEDGEMENTS

The research was carried out due to the support provided by the Miniatura grant, No. 2022/06/X/ST8/00656, National Science Centre, POLAND.

REFERENCES

[1] PN-EN 1993-1-1, Eurocode 3: Design of steel structures – Part 1-1: General rules and rules for buildings, 2005.

[2] A. Biegus, "Calculation of lateral bracing for cantilever and multispan girdersc," *Arch. Civ. Mech. Eng.*, vol. 13, pp. 99–103, 2013, doi: 10.1016/j.acme.2012.11.001.

[3] Sz. Pałkowski and M. Piątkowski, "About calculations of roof cross braces," *Eng. Constr.*, vol. 4, pp. 210–213, 2014.

[4] A. Biegus and D. Czepiżak, "Generalized model of imperfection forces for design of transverse roof bracings and purlins," *Arch. Civ. Mech. Eng.*, vol. 18, pp. 267–279, 2018, doi: 10.1016/j.acme.2017.07.002.

[5] D. Czepiżak and A. Biegus, "Refined calculation of lateral bracing system due to global geometrical imperfections," *J. Constr. Steel. Res.*, vol. 119, pp. 30–38, 2016, doi: 10.1016/j.jcsr.2015.12.007.

[6] M. Krajewski, "Analysis of the influence of geometrical imperfections on the equivalent load stabilizing roof truss with lateral

bracing system," *J. Theor. Appl. Mech.*, vol. 62, no. 2, pp. 231–240, 2024, doi: 10.15632/jtam-pl/185163.

[7] E. Hotała, P. Hotała, and M. Zambrowicz, "Safety of lattice purlins under wind or snow loads," in Proc. *LIII Scientific Conference by Committee of Civil and Water Engineering of the Polish Academy of Sciences*, Krynica, 2007, vol. 2, pp. 233–240.

[8] J. Jankowska-Sandberg, "The influence of the lateral brace stiffness located at the compressed chord on the truss buckling loads," in Proc. *Scientific Conference by Committee of Civil and Water Engineering of the Polish Academy of Sciences*, vol. 2, Krynica, 2004, pp. 221–228.

[9] J. Jankowska-Sandberg, *Selected stability problems of arch and truss girders*, Koszalin, Poland: Koszalin University of Technology publishing house, 2013.

[10] P. Iwicki, "Stability of trusses with linear elastic side-supports," *Thin Walled Struct.*, vol. 45, pp. 849–854, 2007, doi: 10.1016/j.tws.2007.08.005.

[11] P. Iwicki, "Sensitivity analysis of critical forces of trusses with side bracing," *J. Constr. Steel. Res.*, vol. 66, pp. 923–930, 2010, doi: 10.1016/j.jcsr.2010.02.004.

[12] J. Jankowska-Sandberg and J. Kołodziej, "Experimental study of steel truss lateral torsional buckling," *Eng. Struct.*, vol. 46, pp. 165–172, 2013, doi: 10.1016/j.engstruct.2012.07.033.

[13] M. Piątkowski, "Experimental research on load of transversal roof bracing due to geometrical imperfections of truss," *Eng. Struct.*, vol. 242, p. 11255, 2021, doi: 10.1016/j.engstruct.2021.112558.

[14] M. Krajewski, "Stability of trusses with elastic side supports," PhD. thesis, Gdansk University of Technology, Poland, 2021.

[15] M. Krajewski and P. Iwicki, "Stability of an imperfect truss loaded by wind," *Eng. Trans.*, vol. 64, no. 4, pp. 509–516, 2016, doi: 10.24423/engtrans.729.2016.

[16] M. Smak M and B. Straka, "Geometrical and structural imperfections of steel member systems," *Procedia Eng.*, vol. 40, pp. 434–439, 2012, doi: 10.1016/j.proeng.2012.07.121.

[17] A. Biegus, "Trapezoidal sheet as a bracing preventing flat trusses from out-of-plane buckling," *Arch. Civ. Mech. Eng.*, vol. 15, no. 3, pp. 735–741, 2015, doi: 10.1016/j.acme.2014.08.007.

[18] M. Gajdzicki and J. Goczek, "Numerical simulation to determine torsional restraint of cold-formed Z purlin," *International Conference on Metal Structures*, Wrocław, 2011, pp. 424–433.

[19] *Femap with NX Nastran*, Instruction manual, Siemens Product Lifecycle Management Software INC., 2009

[20] R.H. Macneal, "A simple quadrilateral shell element," *Comput. Struct.*, vol. 8, pp. 175–183, 1978.

[21] *Zwick/Roell BIAX Z20* strength testing machine, Instruction manual. [Online]. Available: www.zwickroell.com

[22] *Sick* inclinometer, type TMM88A-PKC090, Instruction manual. [Online]. Available: www.sick.com/1073799

[23] *PMX* measurement amplifier, type 1-PX455, Instruction Manual. [Online]. Available: www.hbm.com/de/2981/pmx-modular-measuring-amplifier-system-for-the-iot

[24] *QuantumX* measurement amplifier, type MX840B, Instruction manual. [Online]. Available: www.hbm.com/quantumx

[25] G. Rakowski and Z. Kacprzyk, *Finite element Method in structural mechanics*. Warsaw, Poland: Warsaw University of Technology publishing house, 1993.